Tunable microbubble generator using electrolysis and ultrasound

Younes Achaoui, Khaled Metwally, Damien Fouan, Zoubida Hammadi, Roger Morin, Eric Debieu, Cédric Payan, Serge Mensah

Tunable microbubble generator using electrolysis and ultrasound

Younes Achaoui,[1] Khaled Metwally,[1] Damien Fouan,[1] Zoubida Hammadi,[2] Roger Morin,[2] Eric Debieu,[1] Cédric Payan,[1,a] and Serge Mensah[1]
[1]*Aix Marseille Univ, CNRS, Centrale Marseille, LMA, Marseille, France*
[2]*CINaM, CNRS, Aix-Marseille Université, UMR 7325, Campus de Luminy, Case 913, 13288 Marseille Cedex 9, France*

(Received 2 November 2016; accepted 22 December 2016; published online 6 January 2017)

This letter reports on a method for producing on demand calibrated bubbles in a non-chemically controlled solution using localized micro-electrolysis and ultrasound. Implementing a feedback loop in the process leads to a point source of stable mono-dispersed microbubbles. This approach overcomes the inertial constraints encountered in microfluidics with the possibility to produce from a single to an array of calibrated bubbles. Moreover, this method avoids the use of additional surfactant that may modify the composition of the host fluid. It impacts across a broad range of scientific domains from bioengineering, sensing to environment. [http://dx.doi.org/10.1063/1.4973720]

The consideration of nano and micro bubbles of controlled size shows a growing interest over a wide range of topics in physics and in chemistry. For instance, in fundamental thermodynamics of nuclei growth, the high interfacial curvature affects not only equilibrium quantities such as surface tension but also heat and mass transports.[1–3] Considering micrometric bubbles, the resonant properties (resonant frequency and Q factor) depend on their size, on the physical characteristics of host medium and on the nature of the enclosed gas. For a given size, the measurement of the resonance makes it possible to estimate physical properties of the host medium or of the gas. This concept is well studied and employed in optics[4–6] to build highly precise micro/nano sensors able to locally measure for example acoustic strain,[7] temperature[8] or pressure.[9] In the field of acoustics, the strong impedance contrast between fluid and enclosed gas as well as the huge amplification or absorption properties at resonance find numerous applications. In medicine, impedance contrast is clinically exploited in ultrasonography through the use of contrast agents.[10] Commercial contrast agents are also employed for local drug delivery.[11] Local motion amplification of micro bubbles at resonance is also a way to enhance either the ablative effect of High Intensity Focused Ultrasound[12] or the vascular permeability[13] making tumor tissues more susceptible to chemotherapy. Moreover, the actual topic of "meta screens" takes advantage of super absorption properties of monodisperse bubble's network at resonance.[14,15]

In all of these issues, the mastery of the microbubble size is mandatory. The ability to produce calibrated microbubbles is thus an important requirement. Lee *et al.*[16] investigated several methods to produce microbubbles. They can be classified into stochastic approaches (ultrasonication, excimer laser ablation, or high shear emulsification), forced extrusion methods (membrane emulsification, inkjet printing method, electrohydrodynamic atomization, acoustic forcing and electric fields), template layer-by-layer deposition,[17] and microfluidics methods. The stringent requirements are to precisely control the bubbling frequency, the bubble size and the properties of the coating. Standing out among these are the flow-focusing based microfluidics[18] techniques. Indeed,

[a]Corresponding author: cedric.payan@univ-amu.fr

microfluidics manages astonishing performances in producing well calibrated microbubbles. Depending on the application, the major drawback of the technique lies in the unavoidable addition of surfactant in order to prevent bubble coalescence. For applications in medicine and biology, this surfactant could be considered as a residual chemical harmful substance. Furthermore, in practice, because of the hydrodynamic resistance, low bubble occurrence frequency or even single bubble generation are quite difficult to obtain. We finally recall that devices involving micro channels or microporous materials are not suitable to be used in all situations since they require dedicated clean-room facilities. Recently, a new technique has emerged to produce monodisperse microbubbles based on electrolysis. It has been reported[19,20] that a platinum micro-electrode with a sharp conical tip can give rise to well-localized bubble generation. Furthermore, calibrated microbubbles could be obtained in controlled electrolytes (H_2SO_4, HCL, NaCl acidic solutions using purified water, $1.5 < pH < 4.5$).

This letter presents a significant step forward from the aforementioned method without any extra component added to the solution, nor special chemical control for producing calibrated bubbles. These calibrated bubbles are obtained by exploiting the mechanism of attractive Bjerknes[21] forces induced by ultrasound. Moreover, a feedback loop, which includes real time processing of video-frames, provides high bubble size stability. In this way, based on the control of the electrolytic current and (when it is required) of the ultrasound wave, a reliable point source of calibrated bubbles is realized using standard on shelf electronic equipment.

The experimental setup (Fig.1) contains a conical tip microelectrode etched from a 125 μm platinum wire and a 3 mm diameter carbon rod counter-electrode both immerged in tap water (pH = 7.5). Voltage applied between the electrodes is provided by an Agilent arbitrary waveform generator, followed by a high speed/high voltage amplifier (Falco System WMA-30NN 150 V maximum output with 2000 V/μs slew rate) and an adjustable resistor R. The 5μm-tip shaped electrode is placed within the focal zone of an ultrasonic transducer. All the experiments are monitored using a high-speed camera (photron SA3). When the ultrasonic transducer is not excited, the bubble generation can be compared to that obtained in the study reported by Hammadi *et al.*[19] in the case of controlled electrolyte. Indeed, we also observe that for a fixed frequency, a voltage threshold should be reached before the bubble generation starts (Fig.2). The borders of the domain where the bubble production is well localized at the electrode tip are delineated in the following way. The electrolytic frequency f_E being fixed, increasing the electrolytic tension V_E triggers the production of bubbles at the apex of the electrode. Pursuing the increase of V_E, keeps localized tip production up to a maximum tension value where many bubbles suddenly appear, not only at the apex but also on a large part of the shank surface of the electrode tip. This tension value is the upper limit of localized production. The process is repeated at different frequencies to complete the curves.

But unlike controlled electrolytes where the produced bubbles are intrinsically calibrated, the gas produced in tap-water is portrayed as a string of non-calibrated bubbles although emerging from the micrometer tip (high localization of the produced gas, Fig.3(a)). Then the high frequency ultrasound generator (1 MHz) is turned on to produce a series of repetitive bursts. The repetition rate is set to

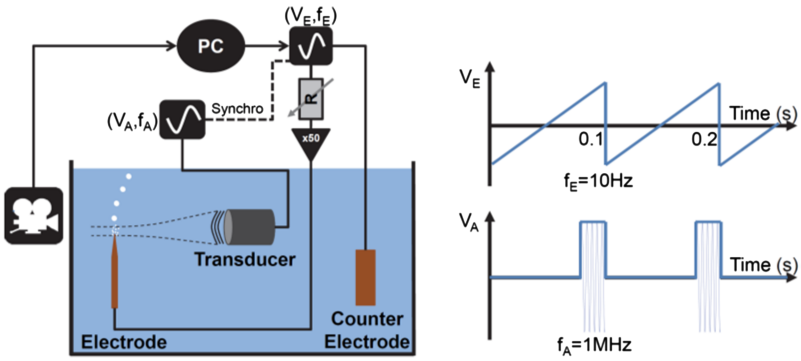

FIG. 1. Experimental setup for the formation of well-calibrated microbubbles by combining water electrolysis and ultrasound. (V_E,f_E) and (V_A,f_A) refer respectively to the voltage and the frequency of the electrolysis and acoustic signals.

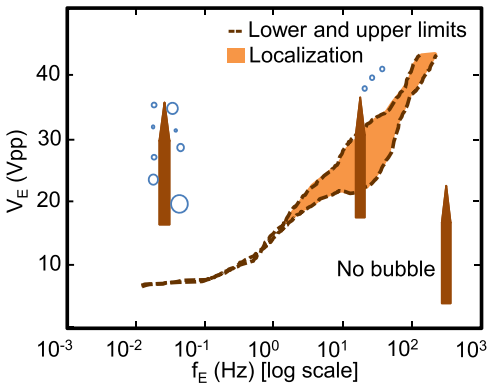

FIG. 2. Experimentally identified region bubble generation localized (not necessarily calibrated) at the tip of the electrode.

10 Hz and matches the electrolytic current frequency (bubbles produced every 100 ms). The acoustic pressure at the focal point of the transducer (Imasonic, Fc = 1 MHz, focal = 90 mm) where the tip has been placed, is adjusted to 6 kPa. In order to limit the extent of the region of coalescence of the bubbles, the electrode tip is placed in the focal zone of the transducer. To properly synchronize the electrolysis signal with the acoustic wave, the time of flight is compensated by assigning the appropriate delay. It is worth noticing that the amplitude of the acoustic pressure is a crucial parameter that determines the strength of Bjerknes forces. Indeed, considering two distant bubbles (*i.e.* the coupling is negligible) in a harmonic pressure field, under the assumption of small amplitudes oscillations, the variations of each of the radii reads:

$$R_i(t) = R_{0i}\left[1 + \frac{\delta R_i}{R_{0i}}\cos(\omega t + \varphi_i)\right]$$

with the response amplitude

$$\delta R_i = \frac{AR_{0i}}{\rho\omega_{0i}^2 R_{0i}^2\left(\left(q_i^2 - 1\right)^2 + 4\,\delta_i^2 q_i^2\right)^{\frac{1}{2}}}$$

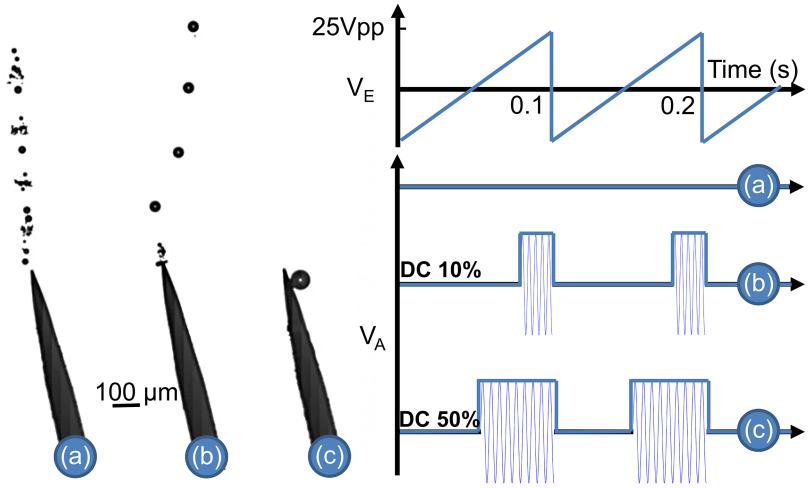

FIG. 3. Example of bubble calibration using acoustics. (a) Bubble production using water electrolysis only ($V_A = 0$). (b) Perfectly calibrated bubbles by means of ultrasounds, one bubble every electrolysis cycle using a duty cycle (DC) of 10%. (c) Possibility to produce bigger bubbles by tuning the acoustic parameters, one bubble every 7 cycles using a duty cycle of 50%. (Multimedia view) [URL: http://dx.doi.org/10.1063/1.4973720.1]

and the phase shift with respect to the pressure filed

$$\varphi_i(t) = \mathrm{Arctg}\frac{2\,\delta_i q_i}{q_i^2 - 1}$$

where A is the amplitude of the forcing pressure field, $q_i = \omega/\omega_{0i}$ the frequency index of bubble i, ρ is the density of the liquid and ω the angular forcing frequency. δ_i is the dimensionless damping coefficient, $\delta_i = \beta_i/\omega_{0i}$, β_i contains viscous, thermal and acoustic damping effects and ω_{0i} is the resonant frequency. The equilibrium radii of the two bubbles are denoted by R_{01} and R_{02}.

When oscillating in a pressure field, two close bubbles are subjected to coupling effects and experience the so-called secondary Bjerknes forces; they attract or repel each other according to whether they oscillate in phase or out of phase, respectively. The magnitude of the force (exerted by the first bubble) acting on the second bubble along the line of the centers reads:[22,23]

$$f_{12} = -2\pi\rho\omega^2\frac{R_{01}^2 R_{02}^2}{r^2}\delta R_1 \delta R_2 \cos\varphi$$

where $\varphi = \varphi_2 - \varphi_1$ is the phase difference between the oscillations of the bubbles. The equation shows that a pair of bubbles which are pulsating in phase (or at phase difference less than $\pi/2$) will engage in an attraction motion that ends with their coalescence. Oppositely, a pair of bubbles which are pulsating at a phase difference φ, such that $\pi/2 \le \varphi \le \pi$, will be subjected to a repulsive force. The simplest way to make bubbles oscillating in phase (attractive force) is to choose a forcing frequency beyond the resonant frequency of every bubble.

This principle is exploited in the process by considering a high frequency (1 MHz) pressure field that induces in phase bubbles oscillations. The efficiency of the procedure is also strongly dependent on the choice of both the ultrasound power and the ultrasound burst length. For instance, when the transmitter acoustic duty cycle is set to 10%, the bursts provide energy that is high enough so that merging of tiny bubbles can occur but at the same time weak enough so that the construction of series of bubbles is not disturbed (Fig.3(b)). The interspacing between bubbles is conditioned by the buoyancy force linked to the bubble radius and the viscosity of the host fluid. When the duty cycle is increased up to 50% and the voltage is kept to the same value, the bubble is trapped by and stick to the electrode (Bjerknes forces) for more than 600 ms, which corresponds to six gas production cycles (Fig.3(c)). In addition, an extra production cycle feeds the bubble growth just before the bubble (subjected to buoyancy force) leaves the electrode region of attraction. The reader is invited to refer to the movie attached to Fig.3 to visualize the effect of ultrasound parameters on the bubble production. Consequently, the bubble radius almost doubles (multiplied by the factor $\sqrt[3]{7} = 1.91$). The bubble repetition rate is therefore not necessarily the same as the frequency of the electrolysis voltage; for instance, in this latter case, it is one seventh of it. However, generally the electrolysis and ultrasound cycle durations are set equal to each other. This is especially required if one looks for the highest bubble rate, which up to the experiments we have conducted reaches up to 200 bubbles per second.

Fig. 4 illustrates the histograms of microbubble radius distributions obtained from several cycles corresponding to Fig.3(a–b). It is shown that without ultrasounds (Fig.4(a)), the natural electrolysis of water using a conical-tip microelectrode gives rise to microbubbles ranging in diameter from 7 µm

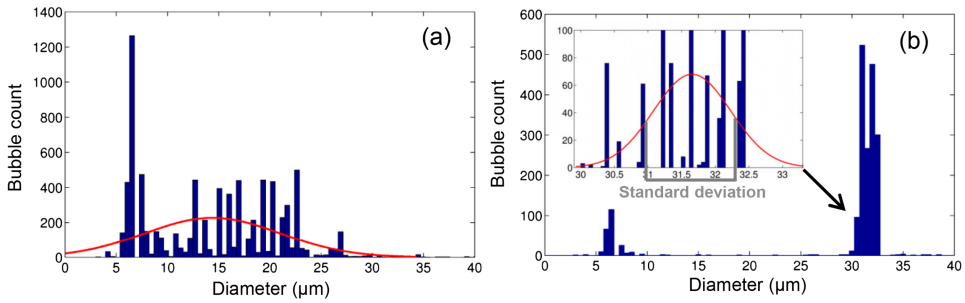

FIG. 4. Microbubble radius histogram for microbubbles generated by water electrolysis. (a) Without generation control. (b) With ultrasound generation control.

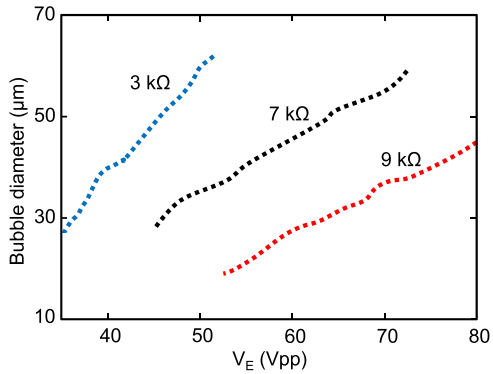

FIG. 5. Produced bubble diameter as a function of applied voltage for different values of the resistance introduced in the electric circuit.

up to 27 µm (case of Fig.3(a)). After ultrasonic induced coalescence (Fig.4(b)), the resulting bubbles have a diameter of 31 µm, with a standard deviation less than 1.5 (case of Fig.4(b)). The values reported in the histogram between 7 µm and 10 µm correspond to pre-coalescing bubbles produced around the tip, which can be observed in Fig.3(b).

In order to underline the link between the volume of gas produced and the applied voltage, we measured the radius of the calibrated bubble produced versus the maximum voltage of the periodic electrical signal. It is shown in Fig.5 that the radius varies linearly with the applied voltage (blue line). Besides, we can notice that, by increasing the resistance in the electrical circuit, we can further increase the sensitivity of the system. By this means, it is possible to achieve easy control of the process and thus to obtain finely tuned chains of monodisperse bubbles.

In order to improve the stability and the reliability of this approach, the control of the bubble production process is implemented using an additional feedback loop, driven by an intuitive graphical user interface in the electrolysis setup. A real-time image processing based on the shape recognition is performed on each video frame and the bubble sizes are estimated. According to the calibration curves shown in Fig.5, the voltage (for a given resistor value) is adjusted to produce the desired bubble radius. The user is required to set the desired value of the bubble radius and the frequency of production. Fig.6 displays an example where the user chose to produce bubbles whose diameters are 60 µm, 70 µm, 35 µm and finally 90 µm. It is worth noting that the acoustic parameters (pressure and burst length) had not been changed. However, for bubble radius beyond 90 µm or below 30 µm, the acoustic parameters should be adapted. Indeed, in the former case, the applied acoustic pressure/burst length becomes insufficient to agglomerate all the bubbles corresponding to the large quantity of gas required; in the second case, the tiny bubble formed remains trapped near the electrode for a long duration during which it goes on growing, exceeding the desired size.

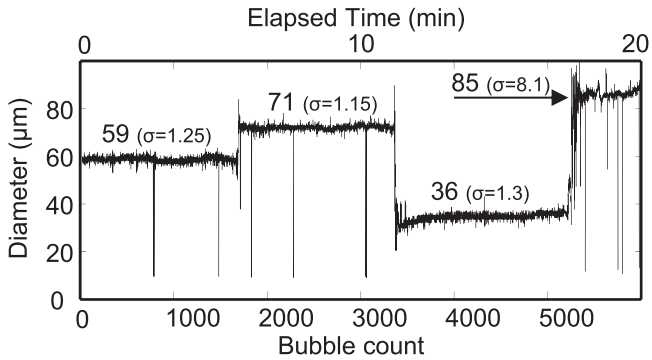

FIG. 6. Stability and reliability of the technique to produce the exact value of the desired bubble diameter. In this example, the user chose to select the radius values 60µm, 70µm, 35µm and 90µm. σ is the standard deviation for each plateau.

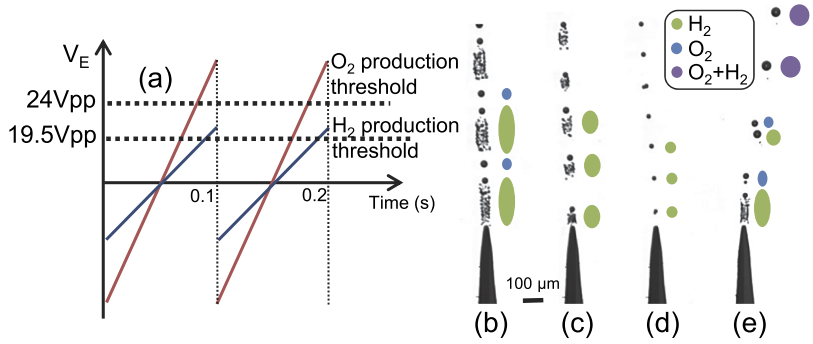

FIG. 7. (a) Applied electric voltage to produce oxygen and hydrogen microbubbles, with the production thresholds (V_E = 24V and 19.5V, respectively). (b) Production of both polydisperse hydrogen and oxygen microbubbles, V_E = 30V. (c) Only hydrogen bubbles are produced, V_E = 23V. (d) Well calibrated bubbles, without ultrasound V_E = 20V. (e) Possibility to separate oxygen and hydrogen bubbles by tuning the ultrasounds, V_E = 28V.

Alternative electrolysis signal organizes the production of hydrogen and oxygen very well. It is well known that in the case of DC electrolysis, oxygen and hydrogen are respectively produced at the cathode and at the anode, depending on the applied voltage. For AC voltage, the sharp electrode plays sequentially the role of the cathode and of the anode and the gas produced is alternatively oxygen and hydrogen. Nevertheless, the hydrogen and oxygen production thresholds (V_E = 19.5V and 24V, respectively) are different. These thresholds are nonetheless highly dependent of the experimental conditions such as the material and the shape (shank angle) of the electrode tip, the conductivity of the solution, etc. Figure 7(a) shows how a 10 Hz AC-ramp signal is used to produce either hydrogen only (blue lines) or both hydrogen and oxygen (red lines). It is also possible to produce oxygen only by adding a positive offset. In Fig. 7(c), it is clearly shown that the big bubbles floating between the bunches of tiny bubbles in Fig. 7(b) disappear suddenly when a maximum voltage below the oxygen production threshold is applied (Fig.7(c)). By further lowering the excitation voltage, it is possible to obtain monodispersed thin hydrogen bubbles without using ultrasounds (Fig.7(d)). Otherwise, the acoustic parameters can be set to be thoroughly adapted for the production of both oxygen and hydrogen (Fig. 7(b)) but with hydrogen bubbles aggregating apart from oxygen bubbles, Fig. 7(e). In that figure, the bunch of tiny bubbles near the electrode is not yet affected by the ultrasounds; the first ultrasound burst results in two separated bubbles (O_2 and H_2) and the second ends with the coalescence of the two bubbles (mixture of O_2 and H_2).

In summary, this letter demonstrates the production of well-calibrated microbubbles in a non-chemically controlled liquid (tap water) under the combined action of microelectrolysis and ultrasound. Applying well-tuned acoustic bursts to the electrode leads to local bubble coalescence and thus results in series of perfectly monodisperse bubbles. Note that an impulse electric signal leads to the production of a single bubble. Moreover, it is reported that the production of pure hydrogen bubbles or hydrogen and oxygen mixture bubbles is possible which could be of interest for energy applications. We further demonstrate that a feed-back loop introduced into the main test bench leads to a stable production of calibrated bubbles and to an easy control of the bubble diameter over a wide range. This method can be implemented for any aqueous solutions that accept the liquid-to-gas phase change with no need for a potential contaminant such as surfactant. It provides a reliable alternative to microfluidics for applications in medicine and biology since bubbles are generated without requiring no chemical additive products. Besides, the absence of any shell around the bubble is of importance in physical domains (for instance in metrology, rheology, fluid dynamics) where the bubble is used as a non-invasive microsensor (measuring the pressure or the viscosity, for instance).

ACKNOWLEDGMENTS

Authors would like to thank Juan Olives for fruitful discussions. Financial support by the Agence Nationale de la Recherche under Grant No. ANR-10-BLAN-0311 (SMART-US) is gratefully acknowledged. Likewise, with financial support from ITMO Cancer AVIESAN (Alliance Nationale

pour les Sciences de la Vie et de la Sante, National Alliance for Life Sciences & Health) within the framework of the Cancer Plan (GRAVITY project).

[1] K. S. Glavatskiy and D. Bedeaux, J. Chem. Phys. **140**, 104708 (2014).
[2] S. Witharana *et al.*, J. Appl. Phys. **112**, 064904 (2012).
[3] S. Maheshwari, M. Van der Hoef, X. Zhang, and D. Lohse, Langmuir (2016).
[4] K. J. Vahala, Nature **424**, 839–846 (2003).
[5] O. Arcizet et al., Phys. Rev. Lett. **97** (2006).
[6] M. Sumetsky, Y. Dulashko, and R. S. Windeler, Opt. Lett. **35**, 898–900 (2010).
[7] Y. Tian, P. Navarro, and M. Orrit, Phys. Rev. Lett. **113**, 135505 (2014).
[8] J. M. Ward, Y. Yang, and S. N. Chormaic, Photon. Technol. Lett. **25**(23), 2350–2353 (2013).
[9] B. Sun et al., Optics Express **23**(3), 1906–1911 (2015).
[10] J. R. Lindner, Nat Rev Drug Discov. **3**(6), 527–532 (2004).
[11] S. Hernot and A. L. Klibanov, Advanced Drug Delivery Reviews **60**(10), 1153–1166 (2008).
[12] Y. Kaneko *et al.*, Eur Radiol. **15**(7), 1415–1420 (2005).
[13] B. Marty *et al.*, J. Cerebr. Blood F. Met. **32**, 1948–1958 (2012).
[14] V. Leroy, A. Strybulevych, M. Lanoy, F. Lemoult, A. Tourin, and J. H. Page, Phys. Rev. B **91**, 020301 (2015).
[15] Y. Li, X. Jiang, B. Liang, J. Cheng, and L. Zhang, Phys. Rev. Applied **4**, 024003 (2015).
[16] M. Lee, E. Y. Lee, D. Lee, and B. J. Park, Soft Matter **11**, 2067–2079 (2015).
[17] V. Leroy, A. Strybulevych, M. G. Scanlon, and J. H. Page, Eur. Phys. J. E **29**, 123–130 (2009).
[18] G. M. Whitesides, Nature **442**, 368–373 (2006).
[19] Z. Hammadi, R. Morin, and J. Olives, Appl. Phys. Lett. **103**, 223106 (2013).
[20] Z. Hammadi, L. Lapena, R. Morin, and J. Olives, Appl. Phys. Lett. **109**, 064101 (2016).
[21] V. Bjerknes, *Die Kraftfelder* (Friedrich Vieweg and Sohn, Braunsweig, 1909).
[22] L. Crum, J. Acoust. Soc. Am. **99**, 3373–3379 (1975).
[23] T. Barbat, J. Fluid Mech. **389**, 137–168 (1999).